

A NON-CONVEX TOTAL GENERALIZED VARIATION MODEL FOR IMAGE DENOISING

Pham Cong Thang*

The University of Danang,
University of Science and Technology
Danang, Viet Nam
pcthang@dut.udn.vn

Tran Thi Thu Thao

The University of Danang,
University of Economics
Danang, Viet Nam
thaotran@due.udn.vn

Dang Hoai Phuong

The University of Danang,
University of Science and Technology
Danang, Viet Nam
dhphuong@dut.udn.vn

Mai Van Ha

The University of Danang,
University of Science and Technology
Danang, Viet Nam
mvha@dut.udn.vn

Article history:

Received 05.12.2022, Accepted 25.05.2023

Abstract

We propose an effective regularization model based on second-order total generalized variation for image restoration with mixed Poisson-Gaussian noise. An efficient alternating minimization algorithm is employed to solve the considered model. Finally, provided numerical results show that our proposed model can preserve more details and get higher image visual quality than recent state-of-the-art methods.

Key words

image denoising, total variation, minimization, mixed Poisson-Gaussian noise.

1 Introduction

Image denoising is an important problem in digital image processing. In practical, the Poisson-Gaussian model can accurately describe the noise present in a number of imaging applications such as astronomy, medicine, biology, etc...[Chouzenoux and et al., 2015; Benvenuto and et al., 2008; Granichin, Erofeeva, and Senin, 2018; Erofeeva, Galyamina, Granichin, et al., 2019]. As is well known, there exists many methods of image denoising of images under Poisson-Gaussian noise, for instance, PURELET [Li, Luisier and Blu, 2018], variance stabilization transforms [Bohra and et al., 2019], unbiased risk estimator [10], contourlet transform and hidden Markov models [Yang and Lee], Total variation (TV) based methods [Li and et al., 2015].

*Corresponding author

Methods based on TV regularization are probably the most popular for mixed Poisson-Gaussian noise removal (TVPG) [Calatroni, Reyes and Schronlieb, 2017; Pham C. Thang, Tran T.T.Thao and et al., 2018b]. More specifically, the TV-based mixed Poisson-Gaussian noise removal model can be expressed as follows (TV model):

$$\mathbf{X}^* = \arg \min_{\mathbf{X}} \left(\int_{\Omega} |\nabla \mathbf{X}| dx + \frac{\lambda}{2} \int_{\Omega} (\mathbf{X} - \mathbf{Y})^2 dx + \beta \int_{\Omega} (\mathbf{X} - \mathbf{Y} \log \mathbf{X}) dx, \right) \quad (1)$$

where \mathbf{Y} is the observed image; $\Omega \subset \mathbb{R}^2$ be bounded open set and \mathbf{X} must be positive almost everywhere over Ω ; λ, β are positive regularization parameters.

For solving the aforementioned optimization problem, many effective numerical techniques can be used, for instance, primal-dual algorithm [Chambolle, 2004], an augmented Lagrangian method [He and et al., 2014; Huang, Ng, and Wen, 2008; Wang and et al., 2008], the split Bregman method [Goldstein and Osher, 2009; Chen and et al., 2015], etc.

As is well known, the TV regularization framework (1) allows the suppression of noise well with sharp edges. Unfortunately, it often leads to the undesired staircase artifacts in the reconstruction, since it tends to transform the smooth regions of the result into piecewise constant regions during iterative process. Many modified TV regularization were proposed to overcome the issue, such as

total generalized variation [Bredies, Kunisch and Pock, 2010; Bredies, Dong and Hintermiller, 2013], non-local total variation [Kayyar and Jidesh, 2018], TV combined with higher-order term [Yang and Zhao, 2019], Euler's elastic model [Zhang and et al., 2017a], mean curvature model [Zhu, Tai, and Chan, 2014; Myllykoski and et al., 2015], fractional order TV [Dong and Chen, 2016; Chowdhury and et al., 2020], overlapping TV [Shi, Han and Liu, 2016; Ding and et al. 2019] and so on.

In this paper, we focus on the total generalized variation (TGV) regularization based image restoration under mixed Poisson-Gaussian noise. Replacing the TV regularization by TGV, the mathematical model for mixed Poisson-Gaussian noise removal can be expressed as follows [Pham et al., 2021](TGV model):

$$\mathbf{X}^* = \arg \min_{\mathbf{X}} \left(TGV_{\alpha}^2(\mathbf{X}) + \frac{\lambda}{2} \int_{\Omega} (Ku - f)^2 dx + \beta \int_{\Omega} (Ku - f \log Ku) dx, \right) \quad (2)$$

where the first term TGV_{α}^2 is the second-order TGV regularization, and the scalar $\alpha = (\alpha_1, \alpha_2)$ is the positive parameter.

The TGV model (2) can perform approximation of image regions with arbitrary order differentiation such as piecewise constant, piecewise affine, piecewise quadratic and so on. Therefore, TGV-based model is better than the TV model in suppressing the staircasing effect with superior performance. However, the TGV regularizer can blur the contours and edges of an image while removing noise, and sometimes even lost some principal details. To improve the edge-preserving ability of TGV, nonconvex TGV (NCTGV) was designed for further avoiding preserving sharp discontinuities and clear contours of the image while alleviating the staircase effect [Ochs and et al., 2015; Zhang and et al., 2017b; Liu, 2021].

In this work, we investigate the non-convex total generalized variation regularization model to remove mixed Poisson-Gaussian noise, which cleverly combines the advantage of TGV regularization with nonconvex penalty (NCTGV):

$$\mathbf{X}^* = \arg \min_{\mathbf{X}} \left(NCTGV_{\alpha}^2(u) + \frac{\lambda}{2} \int_{\Omega} (\mathbf{X} - \mathbf{Y})^2 dx + \beta \int_{\Omega} (\mathbf{X} - \mathbf{Y} \log \mathbf{X}) dx, \right) \quad (3)$$

where $NCTGV_{\alpha}^2$ denotes the non-convex form of TGV_{α}^2 , and its define will be given in the next section.

Our main contributions in this paper are following. We introduce a new total variation model for restoring image with mixed Poisson-Gaussian on the basis of the non-convex penalty with the TGV regularizer. The second important contribution is the proposal of an effi-

cient alternating direction method of multipliers for tackling the resulting variational model. Finally, in comparison with several existing models, experimental results demonstrates the competitive performance of our method for image reconstruction, with respect to restoration accuracy and visual quality.

The rest of this paper is organized as follows. In Section (2), we briefly describe the proposed model for image denoising method with mixed Poisson-Gaussian noise (subsection (2.1)) and establish the proposed algorithm for solving the optimization problem in subsection (2.2). Numerical experiments to illustrate the outstanding performance of our approach are provided in Section (3). Finally, we make conclusions of this work in Section (4).

2 Proposed method

2.1 The denoising model

In this section, we first briefly reviews the fundamental concepts which are relevant to our variational model (see [Bredies, Kunisch and Pock, 2010; Knoll and et al., 2011; Guo, Qin and Yin, 2014; Liu, 2019] for more details)

Let $\Omega \subset \mathbb{R}^d$ be a bound domain, $k > 1$ and $\alpha = (\alpha_0, \alpha_1) > 0$. Then the total generalized variation of second-order with weight α for $u \in L^1(\Omega)$ is defined as the value of the functional:

$$TGV_{\alpha}^2(\mathbf{X}) = \sup \left\{ \int_{\Omega} \mathbf{X} \operatorname{div}^2 \vartheta dx \mid \vartheta \in \mathcal{C}_c^2(\Omega, \mathbb{S}^{d \times d}), \|\vartheta\|_{\infty} \leq \alpha_0, \|\operatorname{div} \vartheta\|_{\infty} \leq \alpha_1 \right\}$$

where d denotes the dimension of images, $\mathcal{C}_c^2(\Omega, \mathbb{S}^{d \times d})$ is the space of compactly supported symmetric $d \times d$ matrix fields, $\mathbb{S}^{d \times d}$ is the set of all symmetric $d \times d$ matrices,

$(\operatorname{div} \vartheta)_i = \sum_{j=1}^d \frac{\partial \vartheta_{ij}}{\partial x_j}$, $(\operatorname{div}^2 \vartheta)_i = \sum_{i=1, j=1}^d \frac{\partial^2 \vartheta_{ij}}{\partial x_i \partial x_j}$. The infinite norms of ϑ and $\operatorname{div} \vartheta$ are given by

$$\|\vartheta\|_{\infty} = \sup_{x \in \Omega} \left(\sum_{i=1, j=1}^d |\vartheta_{ij}|^2 \right)^{\frac{1}{2}}$$

$$\|\operatorname{div} \vartheta\|_{\infty} = \sup_{x \in \Omega} \left(\sum_{j=1}^d |(\operatorname{div} \vartheta)_j(x)|^2 \right)^{\frac{1}{2}}$$

The space of functions of Bounded Generalized Variation is defined as follows:

$$BGV^2(\Omega) = \{\mathbf{X} \in L^1(\Omega) \mid TGV_{\alpha}^2(\mathbf{X}) < \infty\}, \|\mathbf{X}\|_{BGV^2} = \|\mathbf{X}\|_1 + TGV_{\alpha}^2(\mathbf{X}).$$

$BGV^2(\Omega)$ is a Banach space independent of the weight vector α , TGV_{α}^2 is a seminorm and a convex function in $BGV^2(\Omega)$. Subsequently, we denote the spaces $U = \mathcal{C}_c^2(\Omega, \mathbb{R})$, $\mathcal{V} = \mathcal{C}_c^2(\Omega, \mathbb{R}^2)$, and $\mathcal{G} = \mathcal{C}_c^2(\Omega, \mathbb{S}^{2 \times 2})$.

According to [Bredies, Kunisch and Pock, 2010; Knoll and et al., 2011; Guo, Qin and Yin, 2014; Liu, 2019], the discrete TGV_α^2 regularization of u can be formulated as:

$$TGV_\alpha^2(\mathbf{X}) = \min_{\mathbf{W}} \alpha_1 \|\nabla \mathbf{X} - \mathbf{W}\|_1 + \alpha_2 \|\mathcal{E}(\mathbf{W})\|_1 \quad (4)$$

where $\mathbf{W} = (\mathbf{W}_1, \mathbf{W}_2)^T$, $\mathcal{E}(\mathbf{W}) = (1/2)(\nabla \mathbf{W} + \nabla \mathbf{W}^T)$,

$$\nabla \mathbf{X} = \begin{bmatrix} \nabla_1 \mathbf{X} \\ \nabla_2 \mathbf{X} \end{bmatrix} \quad (5)$$

$$\mathcal{E}(\mathbf{W}) = \begin{bmatrix} \nabla_1 \mathbf{W}_1 & \frac{1}{2}(\nabla_2 \mathbf{W}_1 + \nabla_1 \mathbf{W}_2) \\ \frac{1}{2}(\nabla_2 \mathbf{W}_1 + \nabla_1 \mathbf{W}_2) & \nabla_2 \mathbf{W}_2 \end{bmatrix} \quad (6)$$

where $\nabla = (\nabla_1; \nabla_2)$, ∇_1 and ∇_2 are derivative operators in the horizontal and vertical directions, respectively.

Furthermore, by using the non-convex constraints on TGV (4), the non-convex regularization is written as

$$NCTGV_\alpha^2 = \min_{\mathbf{W}} \left(\alpha_1 \mathcal{H}(\nabla \mathbf{X} - \mathbf{W}) + \alpha_2 \mathcal{H}(\mathcal{E}(\mathbf{W})) \right), \quad (7)$$

where \mathcal{H} is non-convex potential function.

2.2 Computational method

In this paper, we introduces a non-convex potential function $\mathcal{H}(q) = \log(1 + \epsilon|q|)$, $\epsilon > 0$, based on the NCTGV regularizer (7), and proposes a novel NCTGV regularized model for mixed Poisson-Gaussian noise removal (3) as follows (NCTGV model):

$$\min_{z,w} \left(\alpha_1 \log(1 + \beta|\nabla \mathbf{X} - \mathbf{W}|) + \alpha_2 \log(1 + \beta|\mathcal{E}(\mathbf{W})|) + \frac{\lambda}{2} (\mathbf{X} - \mathbf{Y})_2^2 + \beta \langle 1, \mathbf{X} - \mathbf{Y} \log \mathbf{X} \rangle \right), \quad (8)$$

In this section, we derive the numerical method for problem (8) in detail. Computationally, we construct the following convex approximation by using the iteratively reweighted l_1 algorithm [Candes, Wakin and Boyd, 2008] as the following surrogate convex optimization problem:

$$\min_{z,w} \left(\alpha_1 \gamma_1^{(k)} (\|\nabla \mathbf{X} - \mathbf{W}\|_1) + \alpha_2 \gamma_2^{(k)} (\|\mathcal{E}(\mathbf{W})\|_1) + \frac{\lambda}{2} (\mathbf{X} - \mathbf{Y})^2 + \beta \langle 1, \mathbf{X} - \mathbf{Y} \log \mathbf{X} \rangle \right), \quad (9)$$

where $\gamma_1^{(k)}$ and $\gamma_2^{(k)}$ are two weights calculated in the k -th iteration as follows:

$$\gamma_1^{(k)} = \frac{\beta}{1 + \beta|\nabla u^{(k)}|} \quad \text{and} \quad \gamma_2^{(k)} = \frac{\beta}{1 + \beta|\mathcal{E}(w^{(k)})|}$$

By the classical augmented Lagrangian multiplier method [Huang, Ng, and Wen, 2008; He and et al., 2014; Goldstein and Osher, 2009; Chen and et al., 2015], we introduce three new variables ($\mathbf{D}, \mathbf{G}, \mathbf{Z}$) and rewrite 9 in the constrained optimization problem as follows:

$$\min_{\mathbf{D}, \mathbf{G}, \mathbf{Z}} \left(\alpha_1 \gamma_1^{(t)} \|\mathbf{D}\|_1 + \alpha_2 \gamma_2^{(t)} \|\mathbf{G}\|_1 + \frac{\lambda}{2} \|\mathbf{Z} - \mathbf{Y}\|_2^2 + \beta \langle 1, \mathbf{Z} - \mathbf{Y} \log \mathbf{Z} \rangle \right) \quad (10)$$

s.t. $\mathbf{D} = \nabla \mathbf{X} - \mathbf{W}$, $\mathbf{G} = \mathcal{E}(\mathbf{X})$, $\mathbf{Z} = \mathbf{X}$,

$$\mathbf{D} = \begin{bmatrix} d_1 \\ d_2 \end{bmatrix} \in \mathcal{V} \quad \text{and} \quad \mathbf{G} = \begin{bmatrix} g_1 & g_3 \\ g_3 & g_2 \end{bmatrix}$$

The augmented Lagrangian functional for the constrained optimization problem (10) is defined as:

$$\begin{aligned} \mathcal{L}(\mathbf{X}, \mathbf{W}, \mathbf{D}, \mathbf{G}, \mathbf{Z}, \rho_1, \rho_2, \rho_3) = & \left(\alpha_1 \gamma_1^{(k)} \|\mathbf{D}\|_1 + \alpha_2 \gamma_1^{(k)} \|\mathbf{G}\|_1 + \frac{\lambda}{2} (\mathbf{Z} - \mathbf{Y})^2 + \beta \langle 1, \mathbf{Z} - \mathbf{Y} \log \mathbf{Z} \rangle \right. \\ & - \langle \theta, \mathbf{D} - \nabla \mathbf{X} + \mathbf{W} \rangle + \frac{\eta_1}{2} \|\mathbf{D} - \nabla \mathbf{X} + \mathbf{W}\|_2^2 \\ & - \langle \xi, \mathbf{G} - \mathcal{E}(\mathbf{W}) \rangle + \frac{\eta_2}{2} \|\mathbf{G} - \mathcal{E}(\mathbf{W})\|_2^2 \\ & \left. - \langle \mu, \mathbf{Z} - \mathbf{X} \rangle + \frac{\eta_3}{2} \|\mathbf{Z} - \mathbf{X}\|_2^2 \right), \quad (11) \end{aligned}$$

where η_1, η_2, η_3 - positive parameters; θ, ξ, μ - with Lagrangian multipliers,

$$|\nabla \mathbf{X}_{i,j}| = \sqrt{(\nabla_1 \mathbf{X}_{i,j})^2 + (\nabla_2 \mathbf{X}_{i,j})^2}$$

, $\nabla_1 \mathbf{X}_{i,j} = \mathbf{X}_{i+1,j} - \mathbf{X}_{i,j}$, $\nabla_2 \mathbf{X}_{i,j} = \mathbf{X}_{i,j+1} - \mathbf{X}_{i,j}$, ($i = 1..M; j = 1..N$).

The minimization method to solve the problem (11) can be expressed as follows:

$$\left\{ \begin{aligned} \mathbf{X}^{(k+1)} &= \arg \min_{\mathbf{X}} \left(- \langle \theta^{(k)}, \mathbf{D}^{(k)} - \nabla \mathbf{X} + \mathbf{W}^{(k)} \rangle + \frac{\eta_1}{2} \|\mathbf{D}^{(k)} - \nabla \mathbf{X} + \mathbf{W}^{(k)}\|_2^2 - \langle \mu^{(k)}, \mathbf{Z}^{(k)} - \mathbf{X} \rangle + \frac{\eta_3}{2} \|\mathbf{Z}^{(k)} - \mathbf{X}\|_2^2 \right), \\ \mathbf{W}^{(k+1)} &= \arg \min_{\mathbf{W}} \left(- \langle \theta, \mathbf{D}^{(k)} - \nabla \mathbf{X}^{(k+1)} + \mathbf{W} \rangle + \frac{\eta_1}{2} \|\mathbf{D}^{(k)} - \nabla \mathbf{X}^{(k+1)} + \mathbf{W}\|_2^2 - \langle \xi, \mathbf{G}^{(k)} - \mathcal{E}(\mathbf{W}) \rangle + \frac{\eta_2}{2} \|\mathbf{G} - \mathcal{E}(\mathbf{W})\|_2^2 \right), \\ \mathbf{D}^{(k+1)} &= \arg \min_{\mathbf{D}} \left(\alpha_1 \gamma_1^{(k)} \|\mathbf{D}\|_1 - \langle \theta, \mathbf{D} - \nabla \mathbf{X}^{(k+1)} + \mathbf{W}^{(k+1)} \rangle + \frac{\eta_1}{2} \|\mathbf{D} - \nabla \mathbf{X}^{(k+1)} + \mathbf{W}^{(k+1)}\|_2^2 \right), \\ \mathbf{G}^{(k+1)} &= \arg \min_{\mathbf{G}} \left(\alpha_2 \gamma_2^{(k)} \|\mathbf{G}\|_1 - \langle \xi^{(k)}, \mathbf{G} - \mathcal{E}(\mathbf{W}^{(k+1)}) \rangle + \frac{\eta_2}{2} \|\mathbf{G} - \mathcal{E}(\mathbf{W}^{(k+1)})\|_2^2 \right), \\ \mathbf{Z}^{(k+1)} &= \arg \min_{\mathbf{Z}} \left(\frac{\lambda}{2} (\mathbf{Z} - \mathbf{Y})^2 + \beta \langle 1, \mathbf{Z} - \mathbf{Y} \log \mathbf{Z} \rangle - \langle \mu^{(k)}, \mathbf{Z} - \mathbf{X}^{(k+1)} \rangle + \frac{\eta_3}{2} \|\mathbf{Z} - \mathbf{X}^{(k+1)}\|_2^2 \right). \end{aligned} \right. \quad (12)$$

with update for $\rho_1^{(k+1)}, \rho_2^{(k+1)}, \rho_3^{(k+1)}$:

$$\begin{cases} \theta^{(k+1)} = \theta^{(k)} + \eta_1 (\nabla \mathbf{X}^{(k+1)} - \mathbf{D}^{(k+1)} - \mathbf{W}^{(k+1)}), \\ \xi^{(k+1)} = \xi^{(k)} + \eta_2 (\mathcal{E}(\mathbf{W}^{(k+1)}) - \mathbf{G}^{(k+1)}), \\ \mu^{(k+1)} = \mu^{(k)} + \eta_3 (\mathbf{X}^{(k+1)} - \mathbf{Z}^{(k+1)}). \end{cases} \quad (13)$$

– **For the X subproblem:** given in (12) as follows:

$$\begin{aligned} \mathbf{X}^{(k+1)} &= \arg \min_{\mathbf{X}} \left(-\langle \theta^{(k)}, \mathbf{D}^{(k)} - \nabla \mathbf{X} + \mathbf{W}^{(k)} \rangle \right. \\ &\quad \left. + \frac{\eta_1}{2} \|\mathbf{D}^{(k)} - \nabla \mathbf{X} + \mathbf{W}^{(k)}\|_2^2 - \langle \mu^{(k)}, \mathbf{Z}^{(k)} - \mathbf{X} \rangle + \frac{\eta_3}{2} \|\mathbf{Z}^{(k)} - \mathbf{X}\|_2^2 \right) \\ &= \arg \min_{\mathbf{X}} \left(\frac{\eta_1}{2} \|\mathbf{D}^{(k)} - \nabla \mathbf{X} + \mathbf{W}^{(k)} - \frac{\theta^{(k)}}{\eta_1}\|_2^2 \right. \\ &\quad \left. + \frac{\eta_3}{2} \|\mathbf{Z}^{(k)} - \mathbf{X} - \frac{\mu^{(k)}}{\eta_3}\|_2^2 \right) \end{aligned}$$

Thus, we get:

$$\begin{aligned} \eta_1 \nabla^T (\nabla \mathbf{X} + \frac{\theta^{(k)}}{\eta_1} - \mathbf{D}^{(k)} - \mathbf{W}^{(k)}) \\ + \eta_3 (\mathbf{X} + \frac{\mu^{(k)}}{\eta_3} - \mathbf{Z}^{(k)}) = 0. \end{aligned}$$

We can rewrite the equation as follows:

$$\begin{aligned} (\eta_1 \nabla^T \nabla + \eta_3) \mathbf{X}^{(k+1)} \\ = \eta_1 \nabla^T (\mathbf{D}^{(k)} + \mathbf{W}^{(k)} - \frac{\theta^{(k)}}{\eta_1}) + \eta_3 (\mathbf{Z}^{(k)} - \frac{\mu^{(k)}}{\eta_3}). \end{aligned} \quad (14)$$

It is obvious that system (14) is linear and symmetric positive definite, therefore $\mathbf{X}^{(k+1)}$ can be efficiently solved by fast Fourier transform (FFT) [Wang and et al., 2008], under the periodic boundary conditions:

$$\mathbf{X}^{(k+1)} = \mathcal{F}^{-1} \left(\frac{\mathcal{F}(\mathbf{S}^{(k)})}{(\eta_1 \mathcal{F}(\nabla^T \nabla) + \eta_3)} \right), \quad (15)$$

where \mathcal{F} and \mathcal{F}^{-1} are the forward and inverse Fourier transform operators, and

$$\mathbf{S}^{(k)} = \eta_1 \nabla^T (\mathbf{D}^{(k)} + \mathbf{W}^{(k)} - \frac{\theta^{(k)}}{\eta_1}) + \eta_3 (\mathbf{Z}^{(k)} - \frac{\mu^{(k)}}{\eta_3}).$$

– **For the W problem:**

$$\begin{aligned} \mathbf{W}^{(k+1)} &= \arg \min_{\mathbf{W}} \left(-\langle \theta^{(k)}, \mathbf{D}^{(k)} - \nabla \mathbf{X}^{(k+1)} + \mathbf{W} \rangle \right. \\ &\quad \left. + \frac{\eta_1}{2} \|\mathbf{D}^{(k)} - \nabla \mathbf{X}^{(k+1)} + \mathbf{W}\|_2^2 - \langle \xi^{(k)}, \mathbf{G}^{(k)} - \mathcal{E}(\mathbf{W}) \rangle \right. \\ &\quad \left. + \frac{\eta_2}{2} \|\mathbf{G} - \mathcal{E}(\mathbf{W})\|_2^2 \right) \\ &= \arg \min_{\mathbf{W}} \left(\frac{\eta_1}{2} \|\mathbf{W} + \mathbf{D}^{(k)} - \nabla \mathbf{Z}^{(k+1)} - \frac{\theta^{(k)}}{\eta_1}\|_2^2 \right. \\ &\quad \left. + \frac{\eta_2}{2} \|\mathcal{E}(\mathbf{W}) - \mathbf{G}^{(k)} + \frac{\xi^{(k)}}{\eta_2}\|_2^2 \right). \end{aligned}$$

Therefore we get:

$$\begin{cases} \left(\eta_1 (\mathbf{D}_1^{(k)} - \nabla_1 \mathbf{Z}^{(k+1)} + \mathbf{W}_1 - \frac{\theta_1^{(k)}}{\eta_1}) + \eta_2 \nabla_1^T (\nabla_1 \mathbf{W}_1 - \mathbf{G}_1 - \frac{\xi_3^{(k)}}{\eta_2}) \right) = 0 \\ \left(\eta_1 (\mathbf{D}_2^{(k)} - \nabla_2 \mathbf{X}^{(k+1)} + \mathbf{w}_2 - \frac{\theta_2^{(k)}}{\eta_1}) + \eta_2 \nabla_1^T (\frac{1}{2} (\nabla_2 \mathbf{W}_1 + \nabla_1 \mathbf{W}_2) - \mathbf{G}_3 - \frac{\xi_3^{(k)}}{\eta_2}) \right) = 0 \\ \left(\eta_1 (\mathbf{D}_3^{(k)} - \nabla_3 \mathbf{X}^{(k+1)} + \mathbf{w}_3 - \frac{\theta_3^{(k)}}{\eta_1}) + \eta_2 \nabla_2^T (\frac{1}{2} (\nabla_2 \mathbf{W}_1 + \nabla_1 \mathbf{W}_2) - \mathbf{G}_3 - \frac{\xi_3^{(k)}}{\eta_2}) \right) = 0 \\ \left(\eta_1 (\mathbf{D}_4^{(k)} - \nabla_4 \mathbf{X}^{(k+1)} + \mathbf{w}_4 - \frac{\theta_4^{(k)}}{\eta_1}) + \eta_2 \nabla_2^T (\nabla_2 \mathbf{W}_2 - \mathbf{G}_2 + \frac{\xi_2^{(k)}}{\eta_2}) \right) = 0 \end{cases} \quad (16)$$

From the system (16), we have

$$\begin{cases} \left(\eta_1 \mathbf{I} + \eta_2 \nabla_1^T \nabla_1 + \frac{\eta_2}{2} \nabla_2^T \nabla_2 \right) \mathbf{W}_1 + \frac{\eta_2}{2} \nabla_2^T \nabla_1 \mathbf{W}_2 \\ = \eta_1 \left(\nabla_1 \mathbf{X}^{(k+1)} - \mathbf{D}_1^{(k)} + \frac{\theta_1^{(k)}}{\eta_1} \right) \\ + \eta_2 \nabla_1^T \left(\mathbf{G}_1 - \frac{\xi_1^{(k)}}{\eta_1} \right) + \eta_2 \nabla_2^T \left(\mathbf{g}_3 - \frac{\xi_3^{(k)}}{\eta_1} \right) \\ \frac{\eta_2}{2} \nabla_1^T \nabla_2 \mathbf{W}_1 + \left(\eta_1 \mathbf{I} + \frac{\eta_2}{2} \nabla_1^T \nabla_1 + \eta_2 \nabla_2^T \nabla_2 \right) \mathbf{W}_2 \\ = \eta_1 \left(\nabla_2 \mathbf{X}^{(k+1)} - \mathbf{D}_2^{(k)} + \frac{\theta_2^{(k)}}{\eta_1} \right) \\ + \eta_2 \nabla_1^T \left(\mathbf{G}_3 - \frac{\xi_3^{(k)}}{\eta_2} \right) + \eta_2 \nabla_2^T \left(\mathbf{G}_2 - \frac{\xi_2^{(k)}}{\eta_2} \right) \end{cases} \quad (17)$$

We have a system of linear equations (17) in two unknowns $\mathbf{W}_1^{(k+1)}, \mathbf{W}_2^{(k+1)}$:

$$\begin{bmatrix} \mathbf{u} & \mathbf{v} \\ \mathbf{e} & \mathbf{f} \end{bmatrix} \begin{bmatrix} \mathbf{W}_1^{(k+1)} \\ \mathbf{W}_2^{(k+1)} \end{bmatrix} = \begin{bmatrix} \mathbf{s} \\ \mathbf{t} \end{bmatrix} \quad (18)$$

with

$$\begin{aligned} \mathbf{u} &= \left(\eta_1 \mathbf{I} + \eta_2 \nabla_1^T \nabla_1 + \frac{\eta_2}{2} \nabla_2^T \nabla_2 \right), \quad \mathbf{v} = \frac{\eta_2}{2} \nabla_2^T \nabla_1, \\ \mathbf{e} &= \frac{\eta_2}{2} \nabla_1^T \nabla_2, \quad \mathbf{f} = \left(\eta_1 \mathbf{I} + \frac{\eta_2}{2} \nabla_1^T \nabla_1 + \eta_2 \nabla_2^T \nabla_2 \right), \\ \mathbf{s} &= \left(\eta_1 \left(\nabla_1 \mathbf{X}^{(k+1)} - \mathbf{D}_1^{(k)} + \frac{\theta_1^{(k)}}{\eta_1} \right) \right. \\ &\quad \left. + \eta_2 \nabla_1^T \left(\mathbf{G}_1 - \frac{\xi_1^{(k)}}{\eta_1} \right) + \eta_2 \nabla_2^T \left(\mathbf{G}_3 - \frac{\xi_3^{(k)}}{\eta_1} \right) \right), \\ \mathbf{t} &= \eta_1 \left(\nabla_2 \mathbf{X}^{(k+1)} - \mathbf{D}_2^{(k)} + \frac{\theta_2^{(k)}}{\eta_1} \right) \\ &\quad + \eta_2 \nabla_1^T \left(\mathbf{G}_3 - \frac{\xi_3^{(k)}}{\eta_2} \right) + \eta_2 \nabla_2^T \left(\mathbf{G}_2 - \frac{\xi_2^{(k)}}{\eta_2} \right) \end{aligned}$$

Similar to the X subproblem, we can solve problems (18) with fast Fourier transform (FFT), under the periodic boundary conditions:

$$\mathbf{W}^{(k+1)} = (\mathbf{W}_1^{(k+1)}, \mathbf{W}_2^{(k+1)})^T \quad (19)$$

where

$$\mathbf{W}_1^{(k+1)} = \mathcal{F}^{-1} \left(\frac{\mathcal{F}(\mathbf{s}\mathbf{f} - \mathbf{v}\mathbf{t})}{\mathcal{F}(\mathbf{u}\mathbf{f} - \mathbf{e}\mathbf{v})} \right),$$

$$\mathbf{W}_2^{(k+1)} = \mathcal{F}^{-1} \left(\frac{\mathcal{F}(\mathbf{u}\mathbf{t} - \mathbf{e}\mathbf{s})}{\mathcal{F}(\mathbf{u}\mathbf{f} - \mathbf{e}\mathbf{v})} \right).$$

– **For the D and G subproblem:**

$$\begin{aligned} \mathbf{D}^{(k+1)} &= \arg \min_{\mathbf{D}} \left(\alpha_1 \gamma_1^{(k)} \|\mathbf{D}\|_1 \right. \\ &\quad \left. - \langle \theta, \mathbf{D} - \nabla \mathbf{X}^{(k+1)} + \mathbf{W}^{(k+1)} \rangle \right. \\ &\quad \left. + \frac{\eta_1}{2} \|\mathbf{D} - \nabla \mathbf{X}^{(k+1)} + \mathbf{W}^{(k+1)}\|_2^2 \right) \\ &= \arg \min_{\mathbf{D}} \left(\alpha_1 \gamma_1^{(k)} \|\mathbf{D}\|_1 \right. \\ &\quad \left. + \frac{\eta_1}{2} \|\mathbf{D} - \nabla \mathbf{X}^{(k+1)} + \mathbf{W}^{(k+1)} - \frac{\theta^{(k)}}{\eta_1}\|_2^2 \right). \end{aligned}$$

$$\begin{aligned} \mathbf{G}^{(k+1)} &= \arg \min_{\mathbf{G}} \left(\alpha_2 \|\mathbf{G}\|_1 - \langle \xi^{(k)}, \mathbf{G} - \mathcal{E}(\mathbf{W}^{(k+1)}) \rangle \right. \\ &\quad \left. + \frac{\eta_2}{2} \|\mathbf{G} - \mathcal{E}(\mathbf{W}^{(k+1)})\|_2^2 \right) \\ &= \arg \min_{\mathbf{G}} \left(\alpha_2 \gamma_2^{(k)} \|\mathbf{G}\|_1 \right. \\ &\quad \left. + \frac{\eta_2}{2} \|\mathbf{G} - \mathcal{E}(\mathbf{W}^{(k+1)}) - \frac{\xi^{(k)}}{\eta_2}\|_2^2 \right). \end{aligned}$$

The solution of the subproblems can readily be obtained by applying the soft thresholding operator [Michelli, Shen and Xu, 2011]:

$$\mathbf{D}^{(k+1)} = \text{Shrink}(\nabla u^{(k+1)} - w^{(k+1)} + \frac{\theta^{(k)}}{\eta_1}, \frac{\alpha_1 \gamma_1^{(k)}}{\eta_1}), \quad (20)$$

$$\mathbf{G}^{(k+1)} = \text{Shrink}(\mathcal{E}(w^{(k+1)}) + \frac{\xi^{(k)}}{\eta_2}, \frac{\alpha_2 \gamma_2^{(k)}}{\eta_2}). \quad (21)$$

where $\text{Shrink}(y, \varphi) = \frac{y}{|y|} \cdot \max(|y| - \varphi, 0)$.

– **The Z subproblem:**

$$\begin{aligned} \mathbf{Z}^{(k+1)} &= \arg \min_{\mathbf{Z}} \left(\frac{\lambda}{2} (\mathbf{Z} - \mathbf{Y})^2 + \beta \langle \mathbf{1}, \mathbf{Z} - \mathbf{Y} \log \mathbf{Z} \rangle \right. \\ &\quad \left. - \langle \rho_3^{(k)}, \mathbf{Z} - \mathbf{X}^{(k+1)} \rangle + \frac{\eta_3}{2} \|\mathbf{Z} - \mathbf{X}^{(k+1)}\|_2^2 \right) \\ &= \arg \min_{\mathbf{z}} \left(\frac{\lambda}{2} (\mathbf{Z} - \mathbf{Y})^2 + \beta \langle \mathbf{1}, \mathbf{Z} - \mathbf{Y} \log \mathbf{Z} \rangle \right. \\ &\quad \left. + \frac{\eta_3}{2} \|\mathbf{Z} - \mathbf{X}^{(k+1)} - \frac{\rho_3^{(k)}}{\eta_3}\|_2^2 \right). \end{aligned}$$

Therefore, we get:

$$\lambda(\mathbf{Z} - \mathbf{Y}) + \beta(1 - \frac{\mathbf{Y}}{\mathbf{Z}}) + \eta_3(\mathbf{Z} - \mathbf{X}^{(k+1)}) - \rho_3^{(k)} = 0.$$

This equation can be rewritten as follows:

$$(\lambda + \eta_3)\mathbf{Z}^2 - \mathbf{Z}(\eta_3\mathbf{X}^{(k+1)} + \rho_3^{(k)} - \beta + \lambda\mathbf{Y}) - \beta\mathbf{Y} = 0.$$

The solution of $z^{(k+1)}$ is the positive solution given by:

$$\mathbf{Z}^{(k+1)} = \frac{-\mathbf{B} + \sqrt{\mathbf{B}^2 - 4\mathbf{A}\mathbf{C}}}{2\mathbf{A}}. \quad (22)$$

where $\mathbf{A} = \lambda + \eta_3$, $\mathbf{B} = -(\eta_3\mathbf{X}^{(k+1)} + \rho_3^{(k)} - \beta + \lambda\mathbf{Y})$, $\mathbf{C} = -\beta\mathbf{Y}$.

The complete method is summarized in **Algorithm 1**. We need a stopping criterion for the iteration: we end the loop if the maximum number of allowed outer iterations N has been carried out (to guarantee an upper bound on running time) or the following condition is satisfied for some prescribed tolerance ς :

$$\frac{\|\mathbf{X}^{(k)} - \mathbf{X}^{(k-1)}\|_2}{\|\mathbf{X}^{(k)}\|_2} < \varsigma, \quad (23)$$

where ς is a small positive parameter.

Algorithm 1: Alternating minimization method for solving the model (8)

1. Initialize: $\mathbf{Z}^{(0)} = q^{(0)} = \mathbf{Y}$;
 $\mathbf{D}^{(0)} = \mathbf{G}^{(0)} = \mathbf{W}^{(0)} = 0$; $k = 1$
 2. **while** Stopping condition is not satisfied **do**
 3. Compute $\mathbf{X}^{(k+1)}$ according to (15)
 4. Compute $\mathbf{D}^{(k+1)}$ according to (20)
 5. Compute $\mathbf{G}^{(k+1)}$ according to (21)
 6. Compute $\mathbf{Z}^{(k+1)}$ according to (22)
 7. Update $\theta^{(k+1)}$, $\zeta^{(k+1)}$, $\mu^{(k+1)}$ by (13)
 8. $k = k + 1$
 9. **endwhile**
 10. **return** u
-

3 Numerical experiments

In this section, we present several simulation results to illustrate the performance of the proposed model for MPGN removal. To further exhibit the image denoising performance, our method is compared with the TV, TGV regularized convex models. The compared models are implemented by the state-of-the-art alternating minimization algorithm. All experiments were carried out in Windows 10 and Matlab running on a desktop equipped with an Intel Core-i3, 2.1 GHz and 12 GB of RAM.

We terminate the iterations of all tested algorithms with tolerance $\epsilon = 0.0001$. Meanwhile, we take peak signal-to-noise ratio (PSNR), and structural similarity index (SSIM)[Wang and et al., 2004] for the quantitative evaluation. Empirically, all images are processed with the equivalent parameters $\lambda = 0.4$, $\beta = 0.6$, $\eta_1 = 1.2$, $\eta_2 = 1.2$, and $\eta_3 = 1$, which gave the best restoration results. The observed images in our experiments are simulated as follows. Noisy observations are generated by Poisson with some fixed peak $I_{\mathcal{P}}$, and by Gaussian noise with standard deviation $I_{\mathcal{G}}$.

In the first example, we show the image denoising performance of compared method TV, TGV and Our proposed. The original ‘Peppers’ image is sized by 256×256 pixels (Figure 1a). Figure (1)b represent its noisy versions degraded by $I_{\mathcal{P}} = 120$, $I_{\mathcal{G}} = 5$. The restorations by the TV, TGV and our method are presented in Figures (1) (c) – (d). Meanwhile, we show the zoomed-in part of the recovered images in Figure (2). The quantitative comparisons are also reported in Table (1).

Secondly, another standard 8-bit grayscale image ‘Asteroidea’ shown in Figure (2)a. The given image with size 256×256 pixels is contaminated by $I_{\mathcal{P}} = 120$, $I_{\mathcal{G}} = 10$ (Figure 2b). The visual comparison of restored images by compared methods is represented in Figures (2)c – (2)d, respectively. Meanwhile, the quantitative evaluations of the compared methods are reported in Table (2).

In Figure (4), we present the restoration result obtained by compared method for the ‘Parrot’ (Figure 4a, 256×256 pixels). The given image is degraded by $I_{\mathcal{P}} = 60$, $I_{\mathcal{G}} = 5$ (Figure 4b). The details of the original are shown in Figure 4c – d. In next rows of the Figure (4), we represent the restorations and their details by the TV (Figure 4e – g), TGV (Figure 4h – 4j) and our method (Figure 4k – 4m), respectively. The comparisons of quantitative values are provided in Table (3) in more detail.

Finally, we test the performance of our method for dealing with color image restoration. The original image ‘Lena’ sized by 256×256 is shown in Figure (5)a. The observed image with noisy level $I_{\mathcal{P}} = 60$, $I_{\mathcal{G}} = 10$ is shown Figure (5)b. The details of the original are shown in Figure (5)c – (5)d. In next rows of the Figure (5), we show the obtained results and their details by the TV (Figure 5e – 5g), TGV (Figure 5h – 5j) and our method (Figure 5k – 5m), respectively. Moreover, we report the quantitative values in Table (4).

Form Figures (1) – (5), we can see that undesirable staircase artifact in our recovered results is fewer than those of the TV method and TGV method. Besides, The comparisons reported in Tables (1) – (4) indicate that our method outperforms other relative methods in restoration precision, especially, in PSNR, SSIM values. It is obvious that our model provides improved visual quality.

4 Conclusions

In this paper, we have investigated non-convex TGV_{α}^2 based model for denoising image corrupted by MPGN. Computationally, an alternating minimization algorithm is employed for solving the proposed optimization problem. Finally, compared with several existing state-of-the-art approaches, the experiments demonstrate competitive performance of the proposed method.

Acknowledgements

This work was supported by The Murata Science Foundation and The University of Danang, University of Science and Technology, code number of Project: **T2021-02-03MSF**.

References

- Pham C.T., Kopylov A.V. (2018). Tree-serial parametric dynamic programming with flexible prior model for image denoising. *Comput. Opt.*, **42** (5), pp. 838–845.
- Le T., Chartrand R., Asaki T.J. (2007). A variational approach to reconstructing images corrupted by Poisson noise. *Journal of Mathematical Imaging and Vision*, **27**, *J. Math. Imaging Vis.*, **27** pp. 257–263.
- Jeziarska, A., Chaux C., Pesquet, J.C., Talbot, H. (2011). An EM approach for Poisson-Gaussian noise modeling. *19th Eur. Signal Pr. Conf. (EUSIPCO)*, Barcelona, Spain, pp. 2244–2248.
- Jeziarska A., Chaux C., Pesquet J.C., and Talbot H. (2014). Iterative Poisson-Gaussian noise parametric estimation for blind image denoising. *IEEE Int. Conf. Image Proc. (ICIP 2014)*, Paris, France, pp. 2819–2823.
- Li J., Luisier F., Blu T. (2018). PURE-LET Image Deconvolution. *IEEE Trans. Image Process.*, **27** (1), pp. 92–105.
- Li J., Shen Z., Yin R., Zhang X. (2015). A reweighted method for image restoration with Poisson and mixed Poisson-Gaussian noise. *Inverse Probl. Imaging*, **9** (3), pp. 875–894.
- Chouzenoux, E., Jeziarska, A., Pesquet, J. C., Talbot, H. (2015). A convex approach for image restoration with exact Poisson-Gaussian likelihood. *SIAM J. Imaging Sci.*, **8** (4), pp. 2662–2682.
- Benvenuto F., Camera A.L., Theys C., et al. (2008). The study of an iterative method for the reconstruction of images corrupted by Poisson and Gaussian noise. *Inverse Probl.*, **24** (3), 35016, 23 pages.
- Lanza A., Morigi S., Sgallari F., Wen Y.W. (2014). Image restoration with Poisson-Gaussian mixed noise. *Comput. Methods Biomech. Biomed. Eng. Imaging Vis.*, **2** (1), pp. 12–24.
- Calatroni L., De Los Reyes J., and Schronlieb C. (2017). Infimal Convolution of Data Discrepancies for Mixed Noise Removal. *Journal on Imaging Sciences, SIAM J. Imaging Sci.*, **10** (3), pp. 1196–1233.
- Pham C.T., Gamard G., Kopylov A., Tran T.T.T. (2018). An algorithm for image restoration with mixed noise

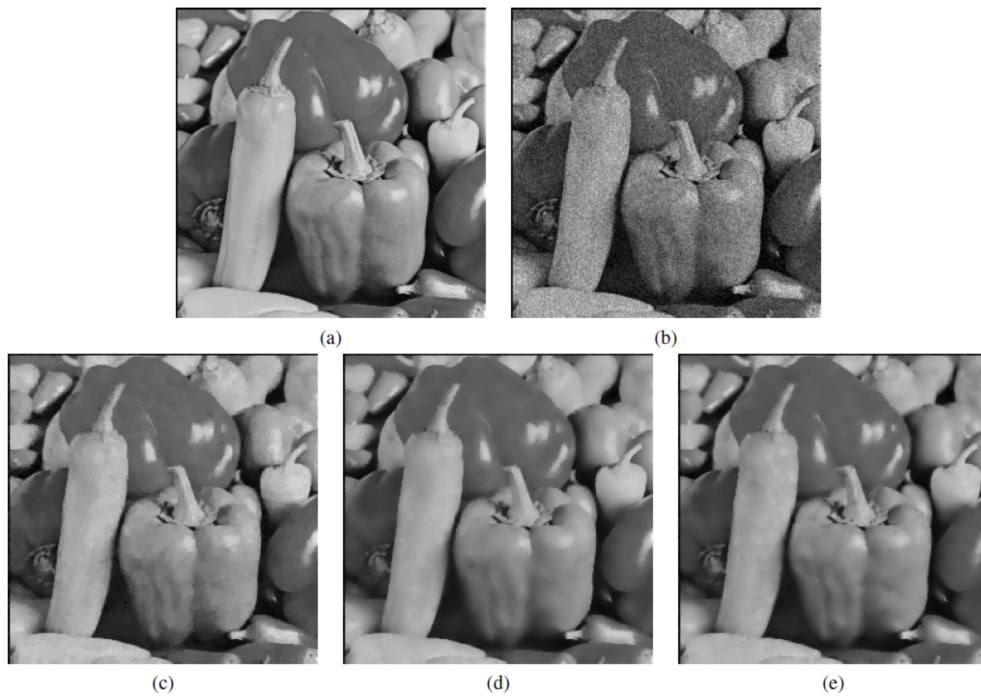


Figure 1. Recovered results for image 'Peppers'. (a) Original image, (b) Noisy image, (c) TV, (d) TGV, (e) Ours

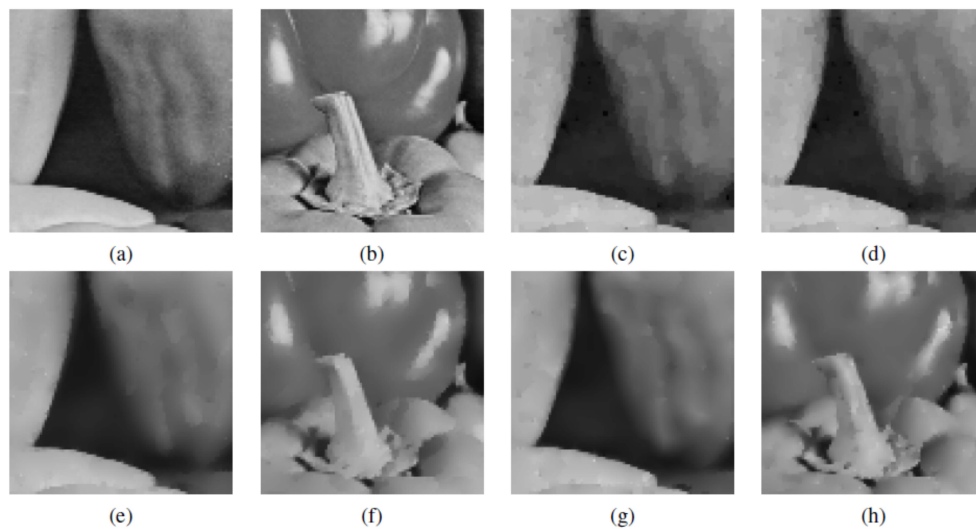


Figure 2. The zoomed-in part of the recovered images in Figure (1). (a) – (b): Original image; (c) – (d): TV, (e) – (f): TGV, (g) – (h): Ours

using total variation regularization. *Turk. J. Electr. Eng. Comput. Sci.*, **26** (6), pp. 2831–2845.

Chambolle A. (2004). An algorithm for total variation minimization and applications. *J. Math. Imaging Vis.*, **20** pp. 89–97.

He, C., Hu, C., Zhang, W., Shi, B. (2014). A Fast Adaptive Parameter Estimation for Total Variation Image Restoration. *IEEE Trans. Image Process.*, **23** (12), pp. 4954–4967.

Huang, Y. M., Ng M. K., Wen Y. W. (2008). A fast total variation minimization method for image restoration. *Multiscale Model. Sim.*, **7** (2), pp. 774–795.

Wang Y., Yang J., Yin W., Zhang Y. (2008). A New Al-

ternating Minimization Algorithm for Total Variation Image Reconstruction. *SIAM J. Imaging Sci.*, **1** (3), pp. 248–272.

Goldstein T., Osher S. (2009). The split Bregman method for L1-regularized problems. *SIAM J. Imaging Sci.*, **2** (2), pp. 89–97.

H. Chen, C. Wang, Y. Song, and Z. Li (2015). Split bregmanized anisotropic total variation model for image deblurring. *J. Vis. Commun. Image Represent.*, **31** pp. 282–293.

Kayyar S. H., Jidesh P. (2018). Non-local total variation regularization approach for image restoration under a

Image Peppers		
$PSNR_{noisy} = 21.0373, SSIM_{noisy} = 0.4826$		
Method	PSNR	SSIM
TV	29.0836	0.8505
TGV	29.4738	0.8600
Ours	30.1279	0.8705

Table 1. Image ‘Peppers’: PSNR values and SSIM measures for noisy images and recovered images

Image Asteroidea		
$PSNR_{noisy} = 17.6200, SSIM_{noisy} = 0.4686$		
Method	PSNR	SSIM
TV	21.9655	0.75351
TGV	24.9899	0.7912
Ours	25.2299	0.8012

Table 2. Image ‘Asteroidea’: PSNR values and SSIM measures for noisy images and recovered images

Image Parrot		
$PSNR_{noisy} = 17.0746, SSIM_{noisy} = 0.3694$		
Method	PSNR	SSIM
TV	23.1239	0.7229
TGV	25.3430	0.7683
Ours	26.2189	0.7887

Table 3. Image ‘Parrot’: PSNR values and SSIM measures for noisy images and recovered images

Image Lena		
$PSNR_{noisy} = 12.8881, SSIM_{noisy} = 0.35075$		
Method	PSNR	SSIM
TV	19.5036	0.6895
TGV	20.1765	0.7279
Ours	21.6813	0.7417

Table 4. Image ‘Lena’: PSNR values and SSIM measures for noisy images and recovered images

Poisson degradation. *J. Mod. Opt.*, **65** pp. 2231–2242.

Zhang J., Chen R., Deng C., Wang S. (2017). Fast linearized augmented Lagrangian method for Euler’s elastica model. *Numer. Math. Theory Methods Appl.*, **10** pp. 98–115.

Zhu W., Tai X.C., Chan T. (2014). A Fast Algorithm for a Mean Curvature Based Image Denoising Model Using Augmented Lagrangian Method. *Lect. Notes Comput. Sci.*, Springer, Berlin, Heidelberg, 8293, pp. 104–118

Myllykoski M., Glowinski R., Karkkainen T., Rossi T.

(2015). A New Augmented Lagrangian Approach for L^1 -mean Curvature Image Denoising. *SIAM J. Imaging Sci.*, **8**(1), pp. 95–125.

Bredies K., Kunisch K., Pock T. (2010). Total generalized variation. *SIAM J. Imaging Sci.*, **3**(3), pp. 492–526.

Bredies K., Dong Y., Hintermüller M. (2013). Spatially dependent regularization parameter selection in total generalized variation models for image restoration. *Int. J. Comput. Math.*, **90**(1), pp. 109–123.

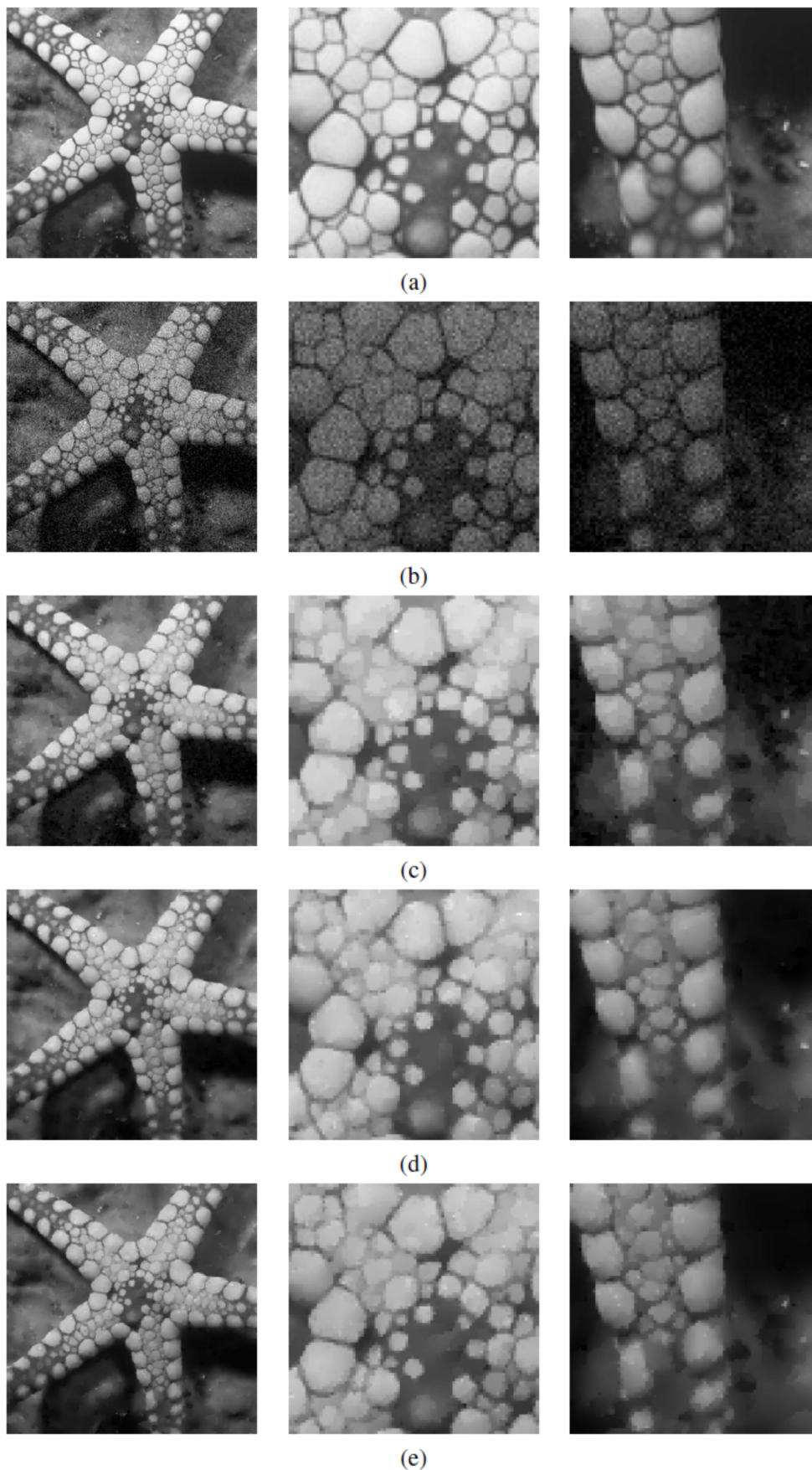


Figure 3. Recovered results for image 'Asteroidea'. (a) Original image, (b) Noisy image, (c) TV, (d) TGV, (e) Ours

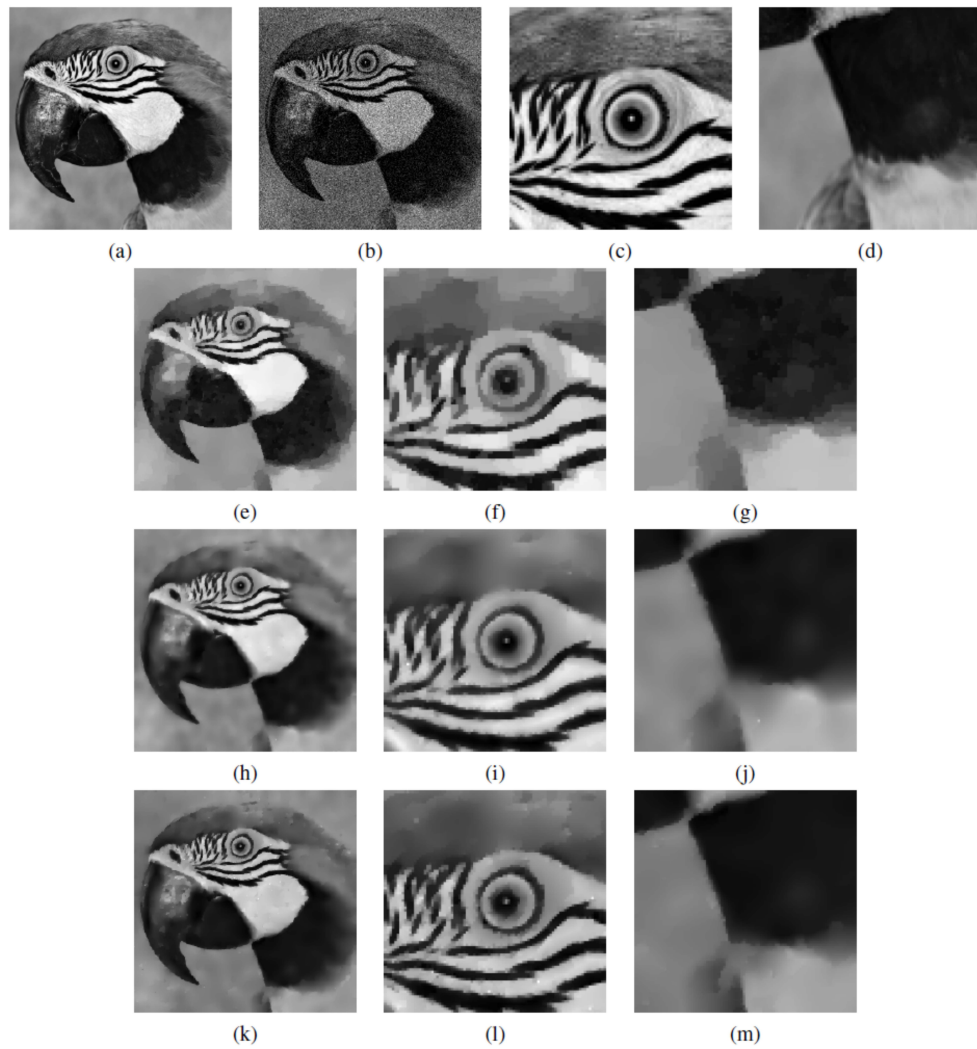


Figure 4. Recovered results for image 'Parrot'. (a) Original image, (b) Noisy image, (c) – (d): details of original; (e) – (g): TV, (h) – (j): TGV, (k) – (m): Ours

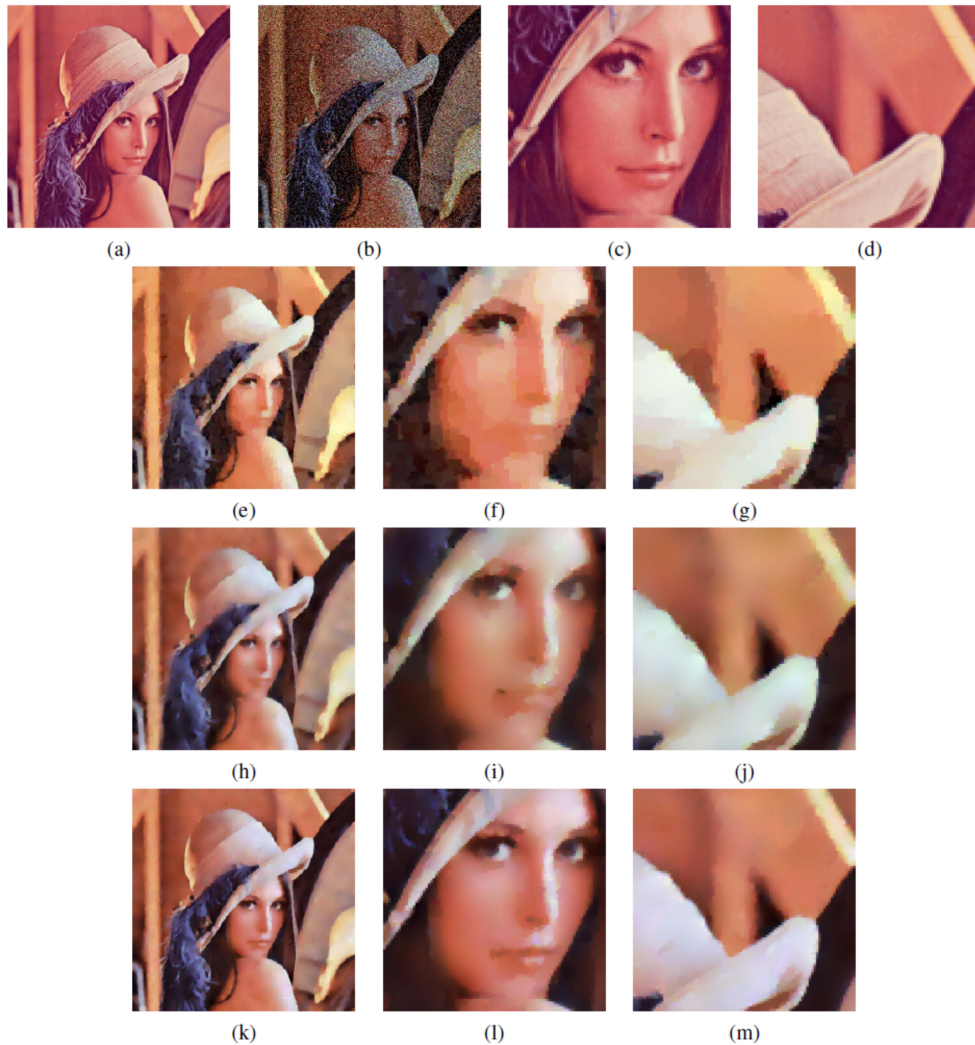


Figure 5. Recovered results for image 'Lena'. (a) Original image, (b) Noisy image, (c) – (d): details of original; (e) – (g): TV, (h) – (j): TGV, (k) – (m): Ours

He C., Hu C., et. al., (2014). An Adaptive Total Generalized Variation Model with Augmented Lagrangian Method for Image Denoising. *Math. Probl. Eng.*, **2014** 157893, 11 pages.

Knoll F., Bredies K., Pock T., Stollberger R. (2011). Second order total generalized variation (TGV) for MRI. *Magn. Reson. Med.*, **65** (2), pp. 480–491.

Guo W., Qin J., Yin W. (2014). A new detail-preserving regularity scheme. *SIAM J. Imaging Sci.*, **7** (2), pp. 1309–1334.

Liu X. (2019). Augmented Lagrangian method for total generalized variation based Poissonian image restoration. *Comput. Math. with Appl.*, **71** (8), pp. 1694–1705.

Pham C.T., Tran T.T.T., Gamard G. (2020). An Efficient Total Variation Minimization Method for Image Restoration. *Informatica*, **31** (3), pp. 539–560.

Micchelli C.A., Shen L., Xu Y. (2011). Proximity algorithms for image models: denoising. *Inverse Probl.*, **27** (4), 0450091, 25 pages.

Wang Z., Bovik A.C., Sheikh, H.R., Simoncelli E.P. (2004) Image quality assessment: From error visibility to structural similarity. *IEEE Trans. Image Process.*, **13** pp. 600–612.

Zhang, H., Tang, L., Fang, Z., Xiang, C., Li, C. (2017). Nonconvex and nonsmooth total generalized variation-model for image restoration. *Signal Process.*, **143** (1), pp. 69–85.

Liu X. (2021). Adaptive regularization parameter for nonconvex TGV based image restoration. *Signal Process.*, **188** 108247, 12 pages.

Ochs P., Dosovitskiy A., Brox T., Pock T. (2015). On iteratively reweighted algorithms for nonsmooth nonconvex optimization. *SIAM J. Imaging Sci.*, **8** (1), pp. 331–372

Yang Y., Zhao D. (2019). An Adaptive Model Combining a Total Variation Filter and a Fractional-Order Filter for Image Restoration. *J. Algorithms Comput. Technol.*, **13** pp. 1–11.

Chowdhury M. R., Zhang J., Qin J., Lou Y. (2020). Pois-

- son image denoising based on fractional-order total variation. *Inverse Probl. Imaging*, **14** (1), pp. 77–96.
- Dong F., Chen Y. (2016). A fractional-order derivative based variational framework for image denoising. *Inverse Probl. Imaging.*, **10** pp. 27–50.
- Shi M. , Han T., Liu S. (2016). Total variation image restoration using hyper-Laplacian prior with overlapping group sparsity. *Signal Process.* , **126** pp. 65–76.
- Ding M., et al. (2019). Total variation with overlapping group sparsity for deblurring images under cauchy noise. *Appl. Math. Comput.*, **341** pp. 128–147.
- Granichin, O., Erofeeva, V., and Senin, I. (2018). Modifying the physical process of ultrasound tomography scanning through compressive sensing. *Cybernetics and Physics*, **7** (2), pp. 66–71.
- Erofeeva V., Galyamina V., Granichin O. (2019). Detection of specific areas and densities for ultrasound tomography. *Cybernetics and Physics*, **8** (3), pp. 121–127.
- Pham C. T., Tran T. T. T., Nguyen T. C., Vo D. H. (2021). Second-order total generalized variation based model for restoring images with mixed Poisson — Gaussian noise. *Inf. Control Sys.*, **2** pp. 20–32.
- Pham C. T., Tran T. T. T., Nguyen T. C., Vo D. H. (2015). Second-order total generalized variation based model for restoring images with mixed Poisson — Gaussian noise. *Inf. Control Sys.*, **2** pp. 20–32.
- Bohra P., Garg D., Gurumoorthy K.S., Rajwade A. (2019). Variance-stabilization-based compressive inversion under Poisson or Poisson–Gaussian noise with analytical bounds. *Inverse Probl.*, **35** (10), 105006, 34 page.
- Candes E.J., Wakin M.B., Boyd S.P. (2008). Enhancing sparsity by reweighted l_1 minimization. *J. Fourier Anal. Appl.*, **14** (5 – 6), pp. 877 – 905.